
PREPRINT

MRzero – Fully automated invention of MRI sequences using supervised learning

Loktyushin A^{1,2*} | Herz K¹ | Dang N³ | Glang F¹ |
Deshmane A¹ | Doerfler A³ | Schölkopf B² |
Scheffler K^{1,4} | Zaiss M^{1,3*}

¹Magnetic resonance center, Max-Planck Institute for Biological Cybernetics, Tübingen, Germany

²Empirical Inference, Max-Planck Institute for Intelligent Systems, Tübingen, Germany

³Friedrich-Alexander Universität Erlangen-Nürnberg (FAU), Neuroradiology, University Clinic Erlangen, Erlangen, Germany

⁴Department for Biomedical Magnetic Resonance, University of Tübingen, Tübingen, Germany

Correspondence

Moritz Zaiss, Max-Planck Institute for Biological Cybernetics, Tübingen, Germany
Email: moritz.zaiss@tuebingen.mpg.de

Funding information

Purpose: A supervised learning framework is proposed to automatically generate MR sequences and corresponding reconstruction without human knowledge on MR strategies. This enables a target-based optimization from scratch, as well as exploration of novel and flexible MR sequence strategies. **Methods:** The entire scanning and reconstruction process is simulated end-to-end in terms of RF events, gradient moment events in x and y, and delay times, acting on the input model spin system given in terms of proton density, T1 and T2, and ΔB_0 . As proof of concept we use both conventional MR images but also binary masks and T1 maps as a target and optimize from scratch using the loss defined by data fidelity, SAR, and scan time. **Results:** In a first attempt, MRzero learns all gradient and RF events from zero, and is able to generate the aimed at target image. Appending a neural network layer to the reconstruction module also arbitrary targets were learned successfully. Experiments could be translated to image acquisition at a real system (3T Siemens, PRISMA) and could be verified in measurements of phantoms and the human brain *in vivo*. **Discussion/Conclusion:** We have developed a fully automated MR

* Equally contributing authors.

A version of this working paper was submitted to MRM for consideration.

sequence generator based on Bloch equation simulations and supervised learning. While we focus on the method herein, having such a differentiable digital MR twin at hand paves the way to a novel way of generating MR sequence and reconstruction solely governed by the target provided, which can be a certain MR contrast, but the possibilities for targets are limitless, e.g. quantification, segmentation, as well as contrasts of other image modalities.

KEYWORDS

digital MR twin, differentiable Bloch equation, AUTOSEQ, automatic MR, supervised learning

1 | INTRODUCTION

Magnetic resonance (MR) images can be created non-invasively using only static and dynamic magnetic fields, and radio frequency pulses. MR imaging provides fast image acquisition which have been clinical feasible only since the discovery of efficient MR sequences[1, 2, 3], i.e., time-efficient application of two building blocks: radio frequency pulses and spatial magnetic field gradients. The proper arrangement of these building blocks is the crucial step for MR sequence development. In the context of MR in medicine, even more important than pure image generation is generation of image contrast. Here MR shows outstanding properties especially in soft tissues, leading to many applications in routine medical imaging with specialized MR sequences for a certain contrast of interest. Here the current paradigm is to alter the MR sequence parameters, guided by insights of physiology and MR physics, in such a way that the generated image shows a certain contrast. This direct relation of the MR image contrast and the actual MR sequence with its many free parameters raises the question if both image and contrast generation can be performed in a completely automatic manner. The principle idea challenging the previous paradigm would be to use a certain desired image contrast as a target, and then automatically generate the MR sequence and reconstruction that is able to generate this contrast using advanced optimization techniques.

The idea of jointly learning acquisition and reconstruction of MR images recently received a lot of attention. Most of the recent work deals with a problem of accelerated imaging, and attempts to learn the optimal k-space undersampling patterns that minimize the scan time, while still obeying scanner limitations and allowing for artifact-free reconstruction [4, 5, 6, 7, 8], which is addressed in more detail in the discussion section. These approaches already link acquisition and reconstruction optimization, although, the mentioned approaches only deal with the sampling pattern aspect of MR measurements, and don't optimize for pulses, gradient forms and timing. Novel approaches target the problem of general sequence learning[9, 10, 11]. The authors propose using deep reinforcement learning to find the optimal sequence satisfying a given loss function. A first approach of automatic sequence generation (AUTOSEQ) for 1D imaging was presented by Zhu et al. based on bayesian deep reinforcement learning [9]. While deep reinforcement learning is highly flexible, it is also costly in terms of computation time, as many parameter paths must be explored before the best path can be found. In contrast, using a gradient based method makes it possible to directly follow the locally steepest gradient path to lower the loss function. Such an approach was also shown in another work of Zhu et al. using auto-differentiation [12]. In the first approach 1D images could be generated based on classic Fourier transform. In the

second approach, only single pixel (OD) evaluations were shown, but with full quantification of Bloch parameters. Another recent sequence generating approach with a completely different target formulation was introduced by Walker-Samuel [10]. Here sequence parameters were also updated using deep reinforcement learning but the task was not to generate an image directly, but to guess a geometric shape in the scanner. Interestingly, by solving this simple task the agent was then able to generate an edge detector.

In the present work we suggest an automatic sequence and simultaneous reconstruction generator framework, *MRzero*, based on supervised learning and a fully differentiable MR simulation. This enables gradient descent in the hyper-parameter space, as well as efficient generalization using many input and target samples. We show how basic image encoding as well as artifact suppression and SAR minimization can be achieved. Furthermore we show how arbitrary target images can be used when using a neural network layer added to the reconstruction, and simultaneously how possible overfitting can be tackled in an efficient manner. *MRzero* does the optimization in a simulation environment, i.e. a differentiable digital twin of the MR system. However, the obtained sequences were implemented on a real clinical MR system and scanned both *in vitro* and *in vivo*. The current work focuses on developing a paradigm for automatic creation of sequences, and as such focuses on the novelty and potential of the method rather than individual results: no fundamentally new sequence/reconstruction method is presented under the scope of this paper.

2 | MATERIAL AND METHODS

In this work we address the problem of automated sequence design and optimization. The approach that we propose allows optimization over spatial encoding gradients (2D), excitation flip angles and their phases, and timing of different events within a sequence affecting the relaxation weighting. The optimization is carried out in a "digital twin" environment (implemented in Torch [13]) simulating and mirroring the acquisition of a real MR scanner. Mathematically, the forward simulation amounts to a chain of tensor-tensor multiplication operations that are applied to a tensor $\mathbf{m} \in \mathbb{R}^{N_{vox} \times N_{spins} \times 3}$ describing a current magnetization state (magnetization is a 3-component vector). N_{vox} and N_{spins} constants determine the number of voxels and spins per voxel used for simulation. The forward process is differentiable in all parameters, and supports an efficient analytic derivative-driven non-linear optimization, which is guaranteed to converge to a local optimum. Furthermore, since the simulation in each spin is independent of all other spins, we can massively parallelize the computations over GPU threads with a minimal implementation overhead, relying on efficient libraries such as Torch[13] and Tensorflow[14], which although designed for Deep Learning, are well-suited for our purpose.

Figure 1 outlines the general method pipeline and problem definition. The pipeline consists of two modules: acquisition and reconstruction. The input to the pipeline are the spin system characterization variables and the output is the image. The proposed framework makes it possible to formulate and solve the following optimization tasks:

1. Given the target image/contrast of interest and associated spin system descriptor (PD/T1/T2/B0 defined at each voxel) find optimal sequence parameters that produce the simulation as close as possible to the target in the L2 or L1 norm sense.
2. Augment the task in 1. with additional constraint terms that allow a sequence with certain aspects of interest. I.e. we might want to keep SAR low, prefer shorter scan times, or better SNR.
3. Given multiple targets/spin system descriptor inputs try to find the sequence that implements tasks 1. and 2. generalizing over data statistics of the input/target pairs. Such a task closely resembles supervised learning regression problem, where instead of a neural network we use a scanner function. In this work we generate a synthetic database (more details below) of input/target pairs on which we train the network. The learned reconstruction module is then

applied to real (in-vivo) data never observed during the training.

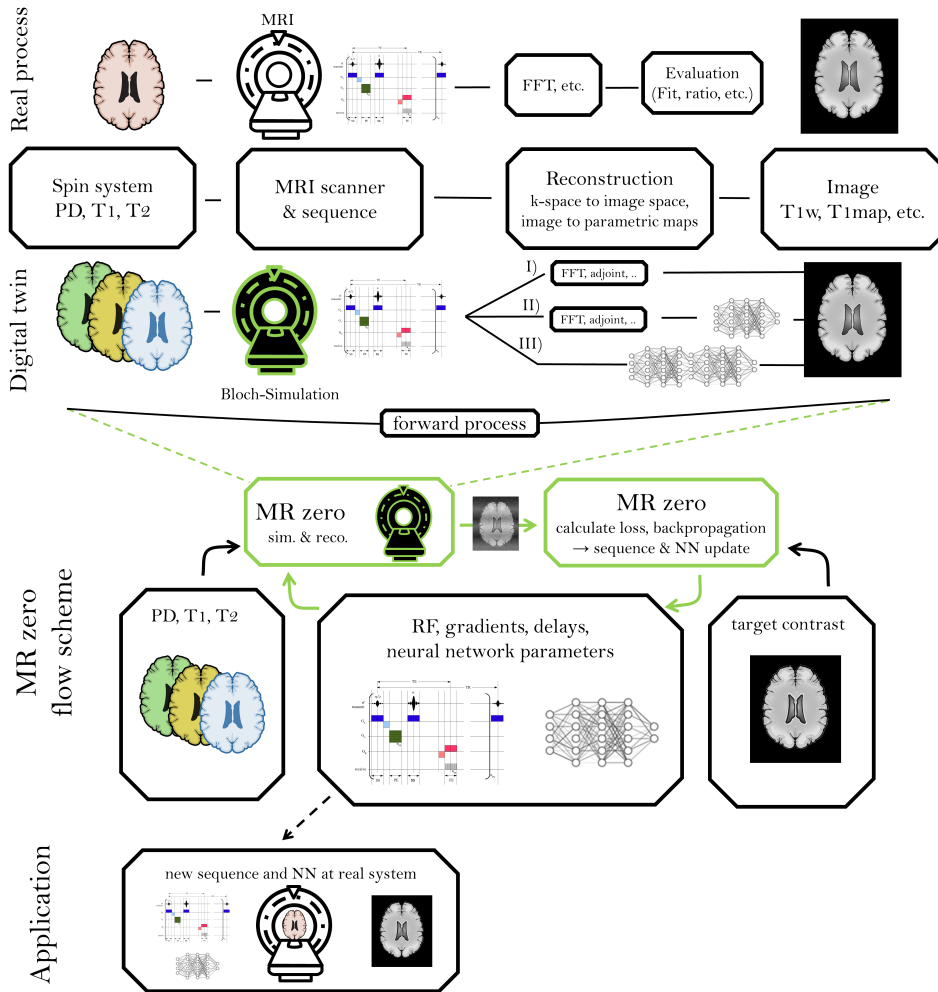


FIGURE 1 MRzero schematic. Figure a) shows the general MRI pipeline from spin system to reconstructed image. For this pipeline a differentiable digital twin implements Bloch equations for signal generation, and for reconstruction either I) conventional reconstruction, II) conventional reconstruction with a neural network appended, or III) a CNN/NN reconstruction is used. This differentiable forward process is a fundamental building block of the MR zero flow scheme (b): The output of MRzero forward process calculation is compared to the target image, analytical derivatives w.r.t. sequence parameters are computed using auto-differentiation, and gradient descent is performed in parameter space to update both sequence and NN parameters. This whole process is repeated until convergence criterion is satisfied subject to loss function imposed on parameters/outputs. (c) Final or intermediate sequences can then be applied at the real scanner using the pulseseq framework. [15]

2.1 | Model description

The forward model is discretized not in time but as a chain of subsequent Bloch actions, each action consisting of an RF event defined by the flip angle α and phase, a gradient precession event defined by the gradient moments \mathbf{g} , a free precession event and a relaxation event with the time variable Δt , and a binary mask if the ADC is open or closed \mathbf{d} , as described in detail in Supporting Information section "Forward Model". Given that each *action* operator in the chain is linear we can concatenate all tensors into a single linear operator *SCANNER*, representing a scanner equation in a compact form:

$$\mathbf{s} = \text{SCANNER}(\alpha, \Delta t, \mathbf{g}, \mathbf{d}) \mathbf{m}_0, \quad (1)$$

where $\mathbf{m}_0 = \hat{\mathbf{e}}_z * PD$ is an initial magnetization state scaled by the proton density at each voxel. Although at each step of the algorithm chain only linear transformations are applied to magnetization tensor, the *action* tensors themselves are composed of the elements that depend in a non-linear way on both sequence parameters and spin system characterization parameters such as T1 and T2.

In our simulation, we distinguish two types of input variables:

1. Scanned object descriptor variables: $PD, T1, T2, R2^*, B0 \in \mathbb{R}^{N_{vox}}$. These parameters are fixed during optimization, and are given as input to the algorithm for a given object sample.
2. Scanner sequence variables: $(\alpha, \Delta t, \mathbf{g}, \mathbf{d})$. Those influence the signal \mathbf{s} output by the scanner operator, and can vary during the optimization process.

Although our model allows for a simple extension to a multi-channel receive/transmit coil setup and parallel imaging, in current proof-of-principle work we use a single receive element in both simulations and real measurements. We also assume uniform receive sensitivity of this element which leads to the fact that PD used in the simulation corresponds to PD times the receive sensitivity map.

2.2 | Reconstruction

In case of Cartesian acquisition, the image reconstruction can be obtained by applying a Hermitian of an orthonormal Fourier transform matrix to the measured signal: $\mathbf{r} = \mathbf{F}^H \mathbf{s}$. In more general case of arbitrary k-space trajectories, it is beneficial to consider the following proxy acquisition equation (we omit relaxation and excitation terms here for the ease of presentation):

$$s_{r,a} = d_{r,a} \sum_{N_{vox}, N_{spins}} \mathbf{m}_{transverse}(x, y) * \exp(i(\sum_{a=0}^{N_{actions}} (g_{x_{r,a}}) * x + \sum_{a=0}^{N_{actions}} (g_{y_{r,a}}) * y))$$

or in matrix form: $\mathbf{s} = \mathbf{E}(\mathbf{g}) \mathbf{m}_{transverse}$, where \mathbf{g} are the gradient moments (integrated gradient events over time) within each action. $\mathbf{m}_{transverse}$ is a 2-component vector describing magnetization state in transverse plane at each voxel before encoding gradients are applied. In case of Cartesian encoding, the matrix \mathbf{E} is equal to a discrete Fourier transform matrix \mathbf{F} . In case of general encoding we approximate the reconstructed image as $\mathbf{r} \approx \mathbf{E}(\mathbf{g})^H \mathbf{s}$. In case the matrix \mathbf{E} is orthonormal the inverse of \mathbf{E} is equal to its Hermitian and the reconstruction is exact.

Using an adjoint of an encoding operator \mathbf{E} makes it possible to avoid using non-uniform Fourier transforms, which require gridding and density compensation. The adjoint of the encoding matrix is differentiable and straightforward to implement. As we show later in the results section, it is also robust in case of small deviations from the uniform k-space sampling. For larger deviations from uniform sampling, as i.e. in radial or spiral imaging, applying the adjoint of the encoding matrix on reconstruction would result in blurring in case the k-space center is oversampled. To resolve this we use an iterative adjoint approach, see Supp. Info Section 'radial MR'.

As elaborated below, the output of the adjoint operator can be the input to a subsequent neural network which we use in one example to generate the final output image. We refer to this form of reconstruction in Figure 1 as reconstruction type II.

2.3 | Target fitting/supervised learning

Lets denote by \mathbf{r} the target image that we want to fit and that is assumed to be given. In case we only optimize for gradient moments we can formulate the following objective function:

$$\mathbf{g}^* = \arg \min_{\mathbf{g}} (\|\mathbf{r} - \mathbf{E}(\mathbf{g})^H \mathbf{E}(\mathbf{g}) \mathbf{m}_{transverse}\|_2^2),$$

Or, in case we optimize for all sequence parameters, using Eq. 1 :

$$\Psi^* = \arg \min_{\Psi} (\|\mathbf{r} - \mathbf{E}(\mathbf{g})^H (\text{SCANNER}(\Psi, \mathbf{m}_0))\|_2^2)$$

where $\{\alpha, \Delta t, \mathbf{g}_{x,y}\} \in \Psi$ are sequence parameters.

We additionally augment the objective function with extra terms that put a penalty on optimized parameters of choice. For example, in case we wish to find a sequence that keeps a moderate SAR the following objective can be used:

$$\Psi^* = \arg \min_{\Psi} (\|\mathbf{r} - \mathbf{E}(\mathbf{g})^H (\text{SCANNER}(\Psi, \mathbf{m}_0))\|_2^2 + \lambda \|\alpha\|_2^2)$$

where the extra term puts an L2 penalty on the magnitude of RF pulses. The λ hyperparameter balances the error made in reconstructing the image and SAR reduction level.

The proposed objective function is non-linear in sequence parameters, since the optimized variables are the arguments of *sin*, *cos* and *exp* functions that form the elements of tensors from Algorithm 1 (see supplementary material). Non-linearity of the objective implies that the loss is non-convex and therefore we are not guaranteed to reach an optimal solution, in fact, depending on initialization and resolution of the image the obtained solution can be arbitrarily poor. To cope with this problem we resort to performing the random restarts of the optimizer with resets of the running optimization step size. It is important to note at this point that although we use the term optimization ubiquitously throughout the paper, the actual goal of this work is not to reach a certain pre-defined "optimality" condition (i.e. being better than existing sequences, or finding a "perfect" solution to a certain problem) but rather to drive the optimized sequence towards a solution that approximates the target of interest. Optimization is performed using the optimizer Adam[16]. The step parameter of Adam is varied from high to low values over the course of the optimization to promote exploration in the beginning and convergence and lack of oscillations at the end. Normally, around 1000 iterations are required to converge to an acceptable result.

2.3.1 | Supervised learning with sparse synthetic training set approach

To avoid overfitting artifacts, we can define an entire set of target/input pairs, and try to learn a scanner function that minimizes the combined error over all training pairs.

$$\Psi^* = \arg \min_{\Psi} \left(\sum_q^{N_{samples}} \|\mathbf{r}_q - \mathbf{E}(\mathbf{g})^H (\text{SCANNER}(\Psi, \mathbf{m}_{0,q}))\|_2^2 \right),$$

here $N_{samples}$ is the number of input/target pairs in the training set. In this research work, we generate a synthetic database of input/target pairs, where each sample in the dataset represents a scanned object primitive. We define such primitives to be just single voxels of non-zero PD at varying spatial locations (see Figure 5). Additionally, we vary T1/T2/B0 value of each voxel primitive in the dataset. We then make a forward pass subject to a target sequence of choice to produce target images that we want to learn to output. A single voxel approach has a significant computational benefit, since we only need to perform Bloch simulations for spins within a single voxel.

2.3.2 | Neural-network-extension to reconstruction module

We extend the versatility of the reconstruction module by augmenting it with a neural network. As an input to the neural network we use the output of the adjoint operator. Stacking the neural network at the end of the forward process chain makes it possible to model diverse targets such as binary segmentation masks or T1 and T2 maps.

$$\Psi^*, \Theta^* = \arg \min_{\Psi, \Theta} \left(\left\| r - N N_{\Theta} \left(E(g)^H (SCANNER(\Psi, m_0)) \right) \right\|_2^2 + \lambda \|\alpha\|_2^2 \right)$$

The neural network weights Ψ are learned alongside with sequence parameter optimization. To avoid the problem of overfitting and reduce a complexity, purely convolutional neural network architectures can be employed. The first layer of the network can have either two channels (real and imaginary output from adjoint), or non-combined output from the adjoint: number of channels equals to $2 * N_{rep}$.

2.4 | Data acquisition at real MR system

After the full in-silico optimization process, certain intermediate iterations were executed on the real system in phantoms and in vivo. To run sequences on a real MR system the sequence parameters were exported using the pulseseq standard ([15], pulseseq.github.io). Pulseseq files can then be interpreted on a MRI scanner including all necessary safety checks, and were executed on a PRISMA 3T scanner (Siemens Healthineers, Erlangen Germany) using a two channel TxRx CP Head Coil (Quality Electrodynamics, Model No 10606826, Serial No 1025, distributed by Siemens). Raw data is automatically sent back to the terminal and the same reconstruction pipeline as for the simulated data is used for measured image reconstruction. As in the simulation only gradient moments and event times were optimized, during export to the pulseseq format actual gradient events with finite slew rates and amplitude were calculated to realize the demanded gradient moment. To be able to run slice selective experiments, block pulses were substituted during export by 1 ms sinc-shaped pulses with time-bandwidth product of 4, and corresponding slice selection and rephasing gradients.

For phantom scans the resolution phantom of Bruker was used positioned at the iso-center. This phantom was fully characterized for a 50 Hz shim using T1, T2, B1 and B0 mapping to generate the exact same phantom in silico. For proton density (PD) a fully relaxed centric-reordered FLASH [1] image was used, thus the coil sensitivities are actually modelled as PD variation in the simulation. To avoid sequence abortion by the scanner due to exceeding SAR limits and potential peripheral nerve stimulation, we used rather conservative building blocks: RF pulses were always contained in a 2 ms block, normally with 1 ms RF duration. Sampling distance in read was 0.08 ms corresponding to a bandwidth of 195 Hz/px for a resolution of 64. In vivo human measurements were approved by the local ethics board.

This work includes five different experiments. i) Learning of encoding from zero using a GRE image as a target (Figure 2), experiments on the importance and effect of SAR regularization for GRE (ii) and RARE targets (iii), in Figures 3-5. The introduction of a sparse synthetic dataset approach to avoid overfitting and its application to RARE and GRE targets, and (v), the introduction of a neural network in the reconstruction (path II in Figure 1) for direct learning of T1 mapping from scratch (Figure 7). All sequences are discovered using simulated training data only, and after training the methods are applied in both in vitro and in vivo.

3 | RESULTS

In the first example, the target is a Cartesian gradient echo image with constant flip angle of 5 degree, as visible in column 6 of Figure 2. A sequence with 48 acquisitions is initialized with all gradients and flip angles set to zero. An additional SAR penalty was added to the cost function, explained in more detail in next paragraph. The initial state

is still visible in the first iterations (column 1 in Figure 2) showing all line acquisitions collapsed starting from $k = 0$ (Figure 2a) and small flip angles (Figure 2b), leading to a non-encoded image in simulation and real measurements (Figure 2cde). During the training the image error with respect to the target decays from 1000 % to 10 % (Figure 2f) by inventing suitable x- and y-gradient events, as well as non-zero RF amplitudes and phases. This enables better and better image encoding and the structure of the phantom becomes visible after 300 iterations, converging at around 600 iterations. The obtained sequence is non-Cartesian and shows a complex RF pattern, still a good match with the target image in the simulation (Figure 1c) and in the real measurement of the corresponding phantom (Figure 1d). The high coherence between our simulation and the measurement is depicted by very similar intermediate images. Interestingly the sequence generalizes well to an *in vivo* measurement of the human brain at 3T. Thus, Figure 2 shows already the full potential of *MRzero*: the invention of a complete MRI sequence that is applicable for image acquisition at a real 3 T system in phantoms and *in vivo*. Please note that the target image does not have to be necessarily an MR image, also a binary mask can be used as a target as shown in Supporting Figure 1 (more details in supplementary materials).

In Figure 3 we want to show the importance of a SAR regularization. Figure 3a-d shows the previous experiment, but without any SAR penalty (at lower resolution). In this case the optimizer can choose very high flip angles, e.g. multiples of 180 and 360 degrees, to generate the target image. The SAR penalty regularizes the invented sequence in an elegant way: Figure 3e-h shows the outcome of a sequence initialized to the target sequence and optimized only for RF events upon a SAR penalty. The optimizer here lowers flip angles in the outer k-space lines to reduce SAR by 27 % tolerating a small image error. A SAR penalty added to the cost function regularizes the flip angles and leads to a low flip angle solution shown in Figure 3i-l.

While a SAR penalty is normally not necessary for a low-angle GRE sequence, the same approach can be performed for the more SAR intensive RARE sequence shown in Figure 4. Here the refocusing flip angles were optimized using *MRzero* under a strong SAR penalty. In the phantom the RARE sequence shows discernible T2-weighting; given the target, *MRzero* tries to reduce SAR while maintaining the contrast. It turns out that SAR can be reduced to 15 % of the target sequence value without loosing much of image quality or contrast (15 % error). For later iterations the strong SAR penalty leads to too high intensities, and blurry images as *MRzero* only allows larger flip angles for center k-space lines.

Despite the observed generalization to *in vivo* applications, the previous approaches are actually prone to overfitting as only one phantom was used during the training with limited distribution of T1 and T2. To overcome possible overfitting biases we suggest to use a suitable simulation for the organ of interest, thus we repeated the optimization shown in Figure 4, but used a brain phantom for training. Here the contrast is better maintained even at very low SAR values (Figure 5 b), and also the sequence strategy is now different, visible when comparing Figure 5a to Figure 4a. Despite increased blurriness, the T2 contrast between CSF and brain matter can be maintained using only 10 % SAR.

3.1 | Supervised learning with sparse synthetic dataset approach

A more general strategy to overcome possible overfitting is the usage of a larger variety of input and target data during training. This unfortunately would prolong training time proportional to the number of samples. To overcome both, overfitting and long training duration, we introduce an approach that solves both problems: a sparse phantom with only few non-zero pixels is generated to save simulation time. A large database (1024 samples) of such input and target blocks at different positions and with different MR properties was generated and used in the training phase in a randomized manner. Directly applied to the previous SAR restricted RARE, Figures 5f-h show the outcome of this approach dubbed sparse synthetic training set learning. Although the training set only consists of very sparse data (Figure 5g), a sequence scheme (Figure 5f) similar to the case of brain phantom training (Figure 5a) is found, and again

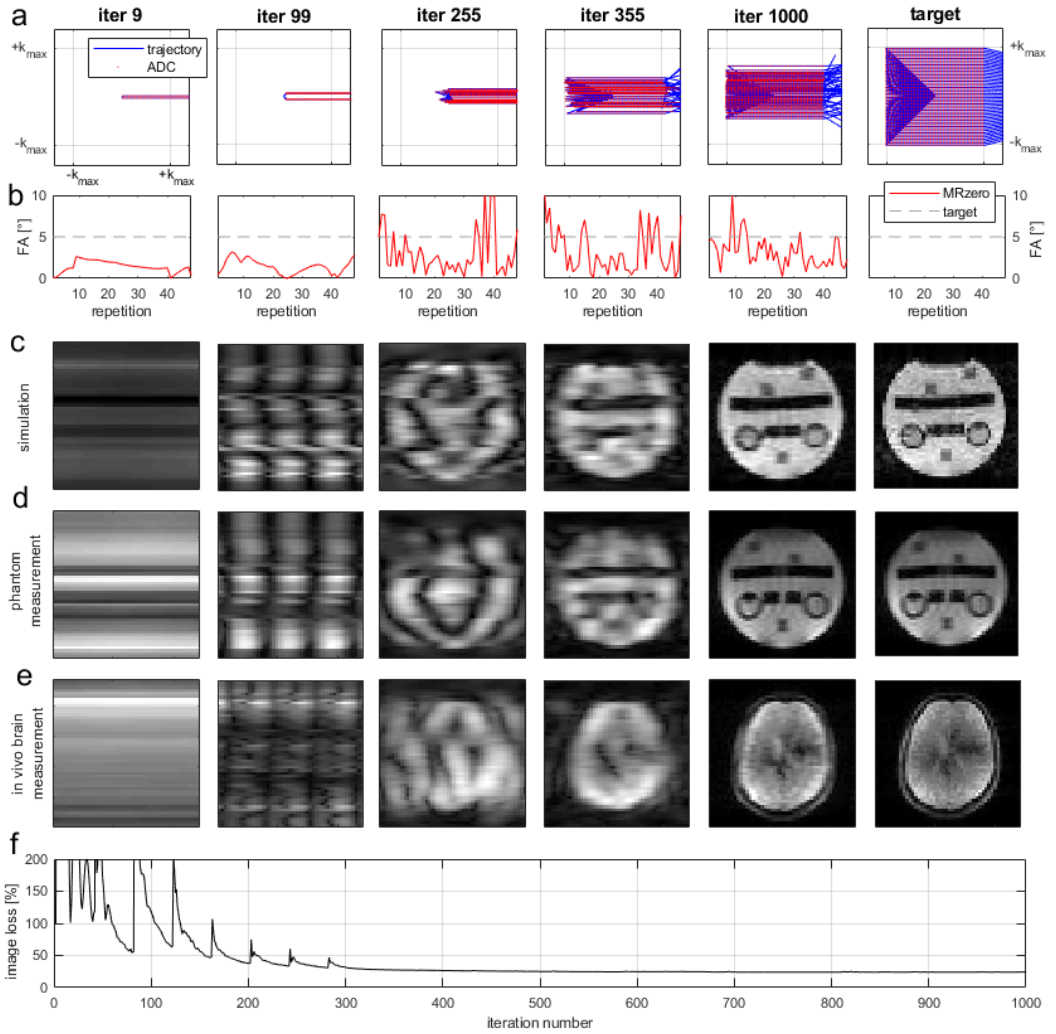


FIGURE 2 Row a: k-space sampling at different iterations, Row b: flip angles over measurement repetitions. Row c: simulation-based reconstruction at different iterations 9, 99, 255, 355, and 1000. row d: phantom measurement, row e: in vivo brain scan. Row f: training error curve. An animated version can be found on www.tinyurl.com/y4z9qlhz. Target sequence: 2D transient gradient- and RF-spoiled GRE, matrix size 48, TR = 20 ms, TE = 3 ms, FA=5 degree.

the contrast is maintained down to SAR values of 10%, with flip angle behavior similar to the work of Hennig et al. [17]. With such a sparse training scheme of our synthetic dataset, spatial encoding strategies can as well be learned, which brings us back to our initial example of Figure 2. Figure 6 shows again the case of Figure 2, using the synthetic dataset approach. It shows that the spatial encoding can as well be learned by a small block that is moved over the FOV during the training iterations. Thus, learning on a sparse synthetic dataset can generally be applied to avoid overfitting. Again,

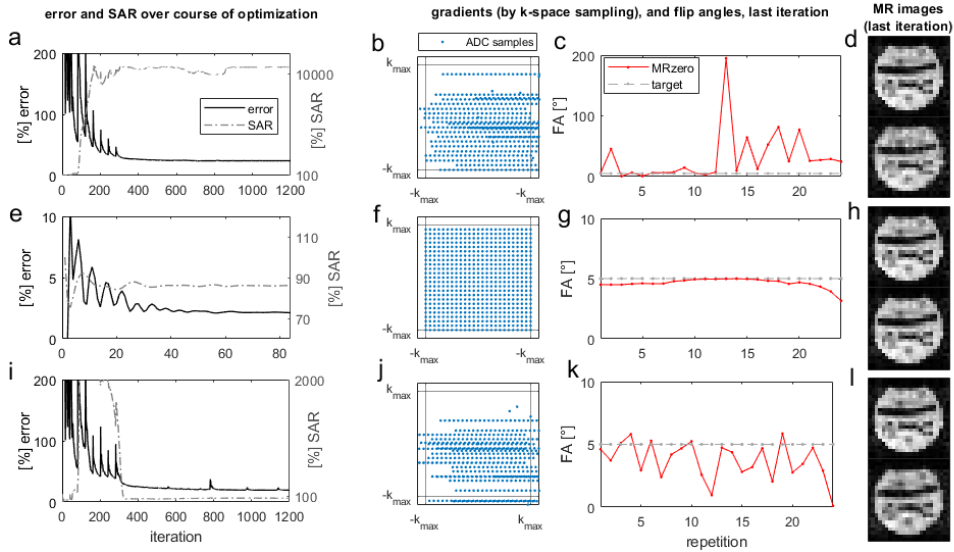


FIGURE 3 SAR regularization. First row: Task as done in Figure 2 with no SAR penalty which leads to a solution with high flip angles. Second row: Task as done in Figure 2 when optimizing only RF events and using a SAR penalty that regularizes the flip angle amplitudes. Third row: Task as done in Figure 2 with gradient and RF optimization upon SAR penalty. a,b,c: Training error curves and relative SAR over optimization steps. b,f,j: k-space sampling at the last iteration. c,g,k: flip angles at the last iteration (red) compared to target flip angles (gray). (d,h,l): Optimized sequence image and target sequence image. Target sequence: 2D transient gradient- and RF-spoiled GRE, matrix size 24, TR = 20 ms, TE = 1.5 ms, FA=5°.

generalization of the learned sequence to both phantom and *in vivo* measurement was proven (Figure 6de).

In a final experiment we performed a joint optimization of sequence and weights of the neural network in the reconstruction module to generate a T1 mapping sequence (case II) in Figure 1). All details of this experiment can be found in the Supporting Information. To reduce parameters we concatenated ten inversion-prepared gradient echo readouts, and set recovery time Trec after each readout and inversion time TI after each inversion pulse to 0 (Figure 7a). Trec and TI were then learned jointly with the pixel-wise neural net with a synthetic dataset approach and T1 values as a target. After several iterations reasonable Trec and TI times were found (Figure 7ab), and the prediction nicely matched literature values, as can be seen in Figure 7cd, which directly shows real *in vivo* data from a 3T brain measurement. Values are slightly higher, compared to a standard inversion recovery experiment, however, learned sequences are shorter.

4 | DISCUSSION

Herein we presented the framework *MRzero* for fully automatic MR sequence generation using arbitrary target images. Sequence learning is performed from zero without using existing knowledge of human MRI experts, but only the underlying laws given by the Bloch equations. In the context of previous MRI developments, where sequence and reconstruction are typically treated as separate problems and are optimized separately, *MRzero* enables flexible combination of sequence parameter optimization and optimization of image reconstruction, by formulating the whole scan

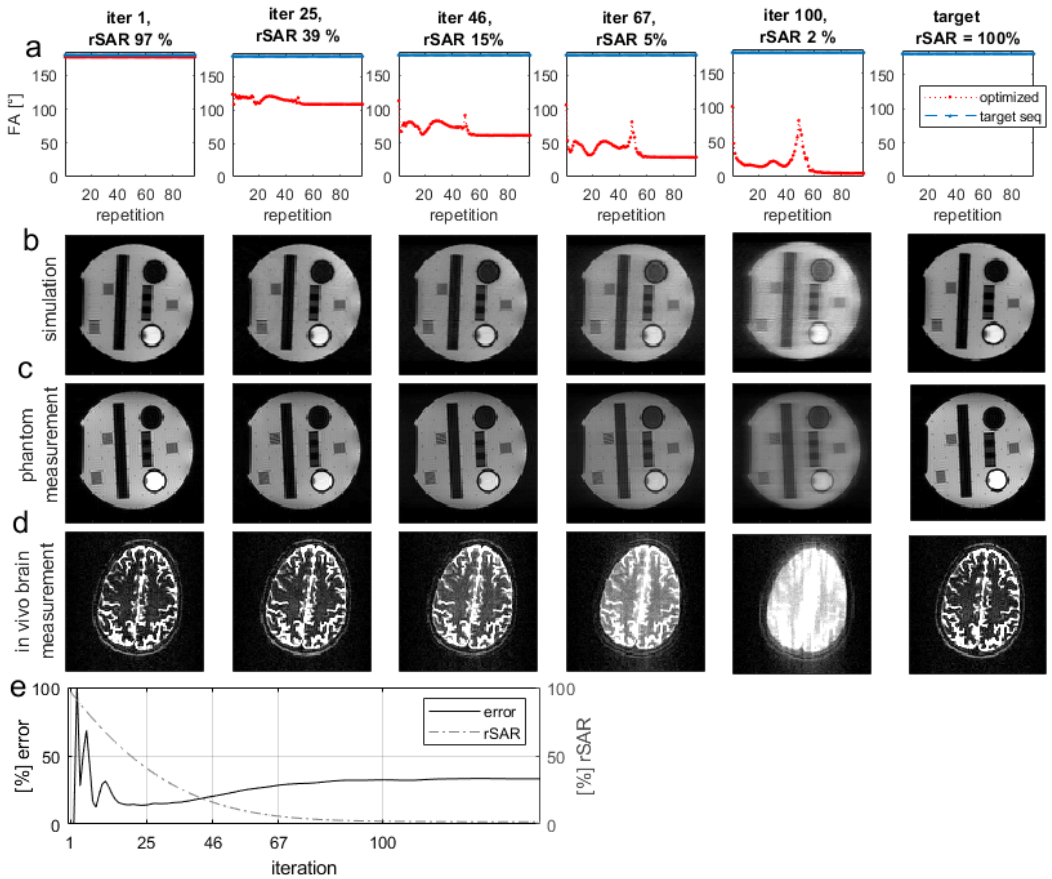


FIGURE 4 RARE sequence: Row a: flip angles at at different iterations, Row b: simulation-based reconstruction at different iterations 1, 25 46, 87 and 100. Row c: phantom measurement. row d: in vivo brain scan. e: training error curve and SAR in percent to the target. Target sequence: 2D RARE, matrix size 96, TA = 0.59 s, TR = 6 ms, excitation FA=90°, refocusing FA=180°.

and image generation process as one differentiable function. The idea of jointly learning acquisition and reconstruction of MRI images is receiving a lot of attention recently. Jin et.al. [4] simultaneously train two neural networks: the first dedicated to reconstruction, and the second to learning the sampling, both being linked with an automatically generated supervision signal created with Monte Carlo tree search. Weiss et.al. [5] propose a fully differentiable end-to-end deep learning-based paradigm to learn an undersampling mask and the reconstructed image jointly. [6] use a supervised learning approach to find the optimal sparse sampling pattern that balances acquisition time and the image quality. Bahadir et.al. [7] use a modified U-Net CNN architecture stacked with a forward model of the undersampling process to jointly learn the undersampling pattern and reconstruction in an end-to-end way. Weiss et.al. [8] make a step further, and formulate their joint acquisition and reconstruction process such that it respects hardware constraints such as peak currents and maximum slew rates of magnetic gradients.

Simultaneous learning of sequence and reconstruction modules makes it possible to come up with measurement protocols that are tailored with respect to a given target contrast. *MRzero* also brings the paradigm shift that happens

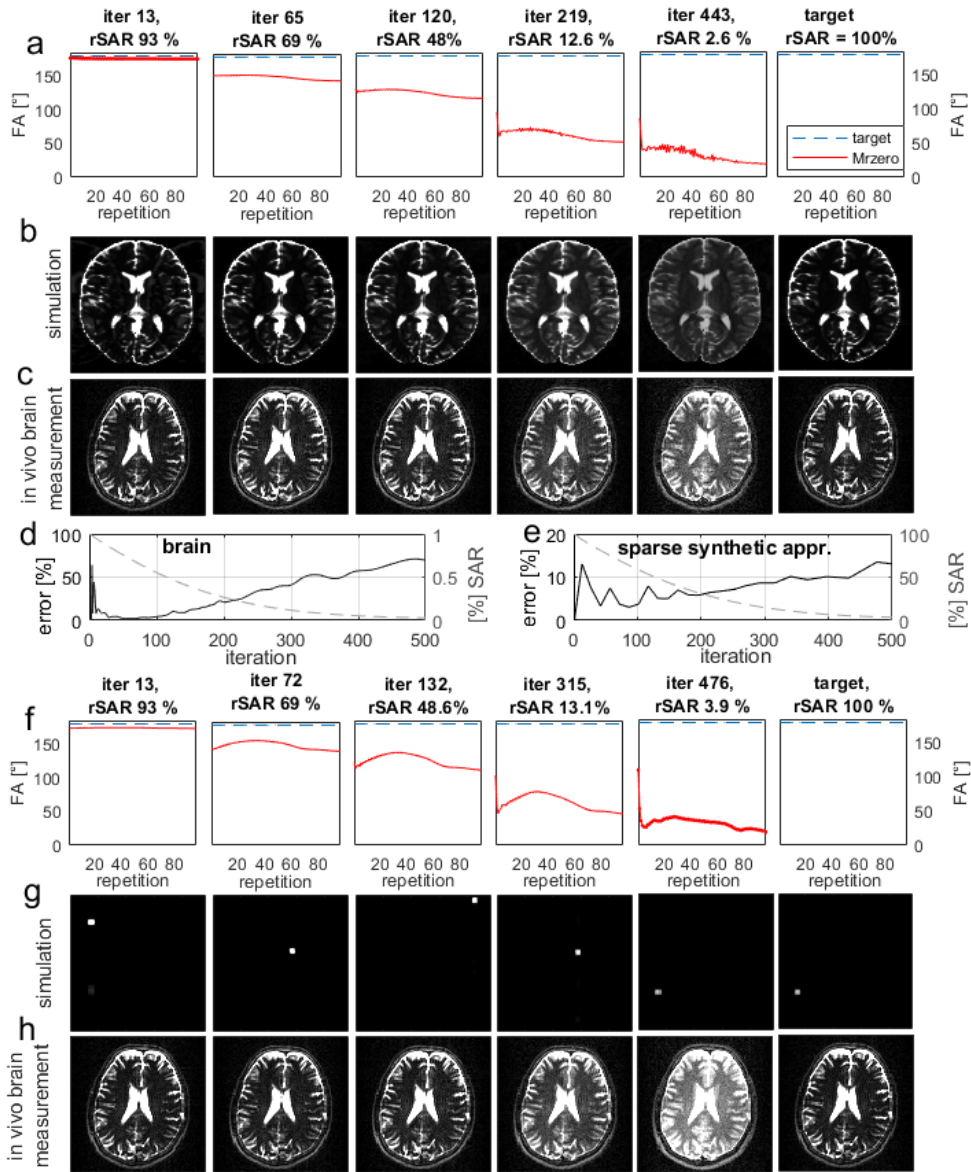


FIGURE 5 a-d: RARE sequence trained on numerical brain phantom. Row a: flip angles at different iterations, Row b: simulation-based reconstruction at different iterations 13, 65 120, 291 and 443. row c: in vivo brain scan. d: corresponding training error curve and SAR in percent to the target. e-h: RARE sequence trained on sparse synthetic database. Row f: flip angles at different iterations, Row g: simulation-based reconstruction at different iterations 13, 72 132, 318 and 476. row h: in vivo brain scan. e: training error curve and SAR in percent to the target for sparse synthetic dataset approach. Target sequence: 2D RARE, matrix size 96, TA = 0.59 s, TR = 6 ms, excitation FA=90°, refocusing FA=180°.

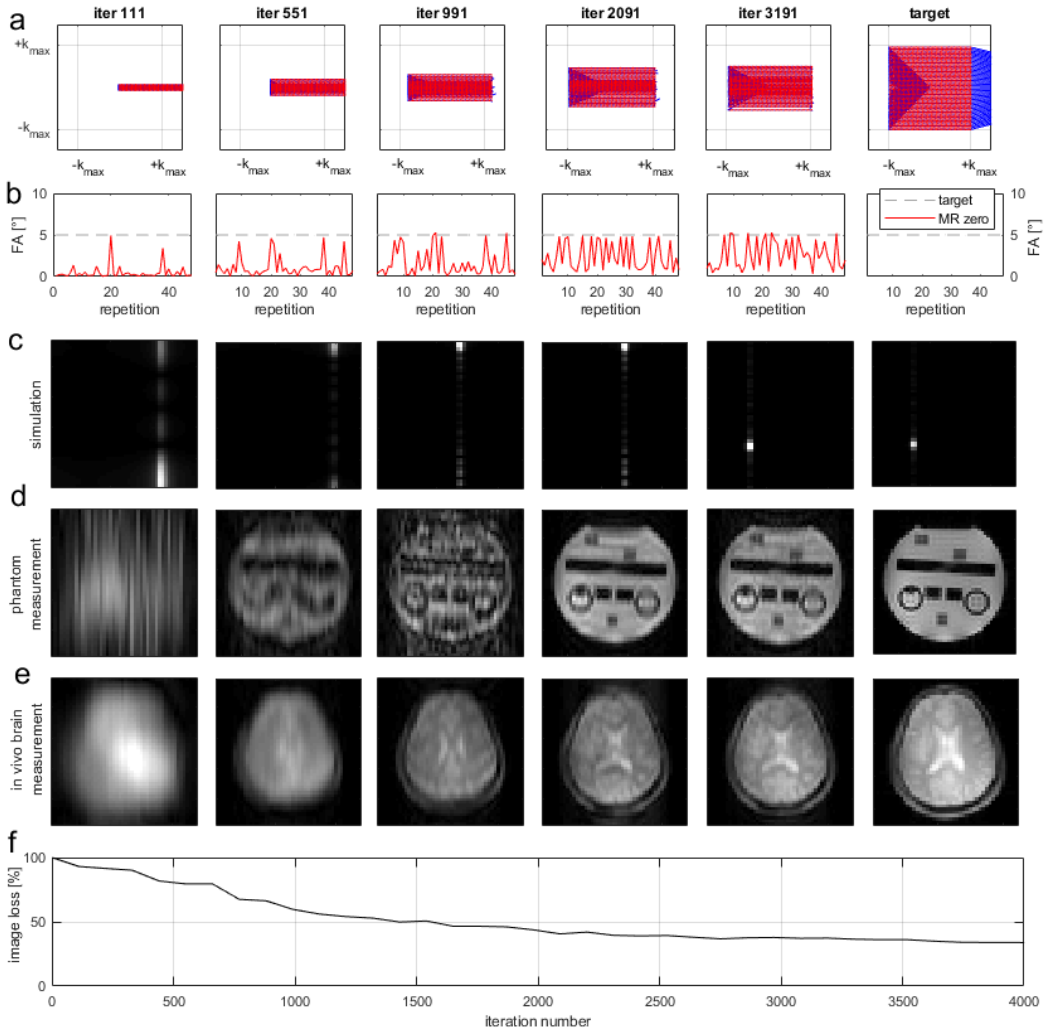


FIGURE 6 GRE sequence: Row a: k-space sampling at different iterations, Row b: flip angles at different iterations. Row c: simulation-based reconstruction (trained on sparse synthetic spins) at different iterations 111, 551 991, 2091, and 3191. Row d: phantom measurement. Row e: in-vivo measurement. f: training error curve. Target sequence: 2D transient gradient- and RF-spoiled GRE, matrix size 48, TR = 20 ms, TE = 3 ms, FA=5°.

currently in many science fields into the world of NMR: instead of engineering sequences or developing reconstruction algorithms, only input and target data is used to automatically learn a solution. In this work, sequence generation is formulated as a supervised learning problem, in contrast to recent developments using reinforcement learning approaches [18, 19]. The term supervised learning refers to the process of learning a function that maps an input to an output, based on example input-output pairs. These pairs are given by (i) the signals of voxels with certain MR properties, generated and encoded using the end-to-end simulation, and (ii) the corresponding target voxel signal. Most

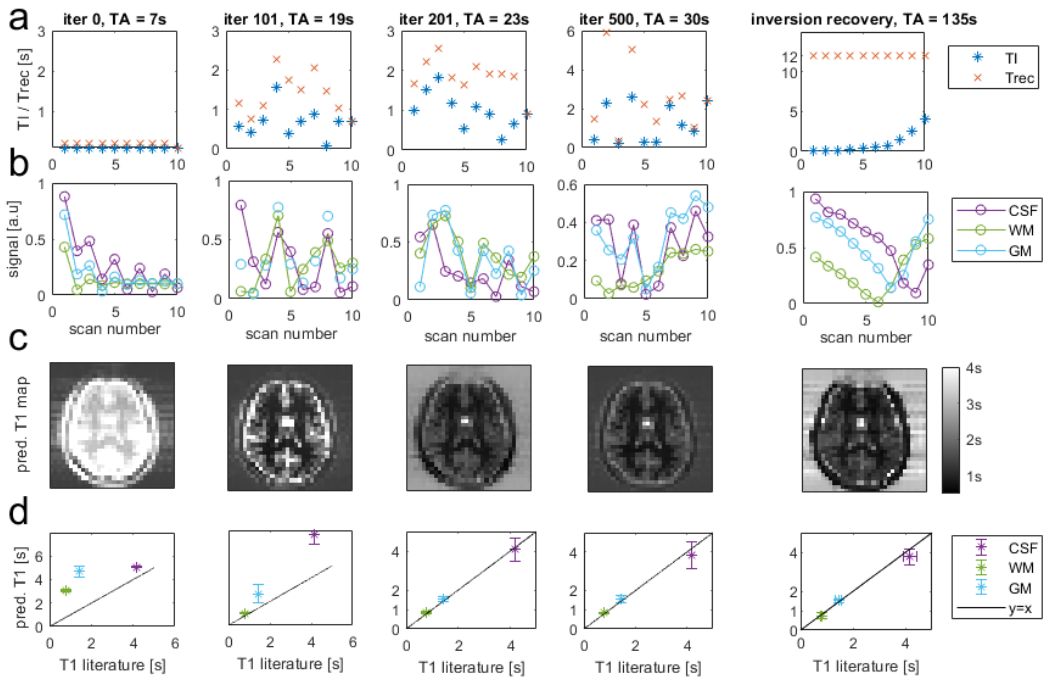


FIGURE 7 Auto-encoding of T1. Strategies here were found using sparse synthetic database approach, but all images are real in vivo scans. (a) shows the different stages of sequence while optimizing T1 and Trec times which were initialized to 0 (a). (b) Corresponding signal evolution for different ROIs. (c) The NN reconstruction predicts the T1 map pixel-wise; the initial step is strongly biased, but after several iterations MRzero adjusts both relaxation and inversion times, until its able to generate a T1map that matches well to literature values at 3 T (d). The rightmost column shows a standard inversion recovery sequence with typical inversion times for reference; signals of this sequence were also evaluated using an adapted neural network. Sequence details: 180 degree inversion prepared 2D transient gradient- and RF-spoiled centric reordered GRE, matrix size 32, TR = 15 ms, TE = 8 ms, FA=5° repeated for 10 times.

of the cases presented in this work are pseudo-supervised (*curve fitting* is a proper term coming from statistics) as e.g. a phantom with only a few different T1 and T2 values was used, thus only few different input and output pairs were available during training. Such small training databases are known to lead to overfitting during the training, which means that the learned sequences can only be faithful to T1, T2 and B0 distributions similar to those used in simulations. Interestingly, for image encoding in GRE-like sequences (Figure 2-3), we did not observe overfitting to be a problem. However, when it comes to flip angle amplitudes in RARE sequences, which have more effect on the actual contrast, overfitting was clearly observed when using different sequence strategies in the simple phantom compared to the brain phantom (Figure 4-5). We addressed overfitting issues by proposing a sparse synthetic training set approach which was composed of single pixels sampled from a database that had similar PD/T1/T2 distributions as the human brain. This approach has the advantage of generality and computation efficiency, but, with real quantitative MR data and using general reconstruction module such as neural networks we can expect better performance. Using neural networks and representative MR image databases, we expect the priors on real image distribution to be implicitly encoded in the weights of the neural network [20].

The problem with using databases of quantitative MR data is that such databases need to be comprehensive and

large, representing all sorts of morphological anomalies. However we think that with the current developments in magnetic resonance fingerprinting (MRF) [21, 22, 23, 24, 25] such large databases will be available in the near future for different organs and field strengths, and then can be used in future extended versions of *MRzero*. Quantitative MR properties can also be used as targets as shown in the T1 quantification experiment (Figure 7). In this experiment we showed that *MRzero* can be treated as a complete auto-encoder and in principle novel MRF paradigms can be explored and optimized autonomously. Previously, many detailed analyses were performed for MRF schedule optimization [26], a first joint optimization of sequence and reconstruction using neural networks was shown for OD by Zhu et al [12]. *MRzero* is able to perform such joint optimization in 2D, following the same approach as shown for T1 mapping, validated by real measurements. We were still using a conventional image reconstruction augmented with a small neural network, though the framework for a CNN based reconstruction would be exactly the same.

4.1 | Implementation of differentiable simulation and reconstruction

Our forward process can be efficiently parallelized with the use of GPUs. The parallelization is carried out over spins and voxels. Indeed, Bloch simulations for each individual spin at each individual voxel, are independent of all other spins at all other voxels, meaning we can run thousands of parallel threads for simulating magnetization evolution at each spin. Although, the forward process is then very efficient to carry out, given multiple repetitions and samples per readout, the simulation can be very lengthy. This is because, tensor-tensor operations need to be performed sequentially, when proceeding through a chain of actions and repetitions. We can somewhat reduce the computational burden by grouping together all actions within the ADC readout at each repetition, and assuming there is no relaxation or phase evolution due to B_0 within each readout chunk. It then makes it possible to compute gradient precession operations efficiently by computing them not sequentially but in parallel.

Our current implementation uses 625 spins per voxel; the high number of spins is required to properly describe transient net magnetization, especially in case of spoiled gradient echo-like sequences. Already for 48×48 voxels this implies more than a million of variables that need to be manipulated at every *action* step, which gives our model a high computational cost. Moreover, transient MR sequences form a sequential chain, that could not be further parallelized. Fortunately, calculation within each time step could be run in parallel for all voxels and all spins within each voxel leading to a single forward/backward pass time for a single 2D image (48×48 voxels \times 625 spins) of around 30 seconds on a Nvidia V100 card. This computation time already assumes a speed-up gained by joining the entire intra-repetition readout block into one tensor operation.

For image reconstruction we employed a differentiable adjoint formalism. Using the adjoint formalism has an important benefit that no regridding is needed but still arbitrary k-space sampling is possible. The adjoint, which is basically a naïve inverse Fourier transform is less efficient compared to an FFT algorithm, but as mentioned above the bottleneck with regard to time is still the Bloch simulation. At the same time, the adjoint formalism when combined with a post-processing neural network module makes it possible to avoid fully connected networks such as those used in AUTOMAP [27]. Instead fully convolutional networks that have fewer parameters and are less prone to overfitting can be used.

4.2 | Real MR measurements

In this work we have dedicated a lot of effort to establish a model in agreement with the outputs from real measurements. Indeed, since the model is used to optimize sequence parameters, such agreement is critical for good performance of the learned sequence. Particularly helpful were intermediate results from optimization chains, where both in simulations and real measurements the same artifacts occur, either because of unbalanced flip angles, inadequate k-space sampling,

or inefficient spoiling. Such cases with artifacts are even more useful than artifact-free clean images since they allow to compare in-silico and real measurements in non-trivial regimes.

While for final applications only the last iteration might be of interest, we cannot stress enough how important it was to check the intermediates for consistency, and how exciting it was to watch the intermediate solutions and images. The implementation using pulseq [15] allowed for a fully integrated solution enabling to dispatch the same sequence to both simulation and real MR scanner. After the signal is produced either on a real or artificial system exactly the same reconstruction process involving the adjoint transform and neural network is applied to the signal.

5 | CONCLUSION

We have developed a fully automated MRI sequence generator based on the Bloch equation simulations and supervised learning. While we focus on basic image generation herein, having such a tool at hand paves the way to novel solutions in generating optimal MR sequences and reconstructions solely governed by the target provided, which could be a certain MR image, but the possibilities for targets are limitless, e.g. quantification, activation, segmentation or contrasts of other image modalities.

ACKNOWLEDGEMENTS

We thank Maxim Zaitsev and his team for developing and sharing pulseq [15]. The research that we have done would not be possible without this versatile and powerful framework. We also thank the authors and developers of pypulseq library [28], the parts of which we used to build a python interface to pulseq.

REFERENCES

- [1] Haase A, Frahm J, Matthaei D, Hanicke W, Merboldt KD. FLASH imaging. Rapid NMR imaging using low flip-angle pulses. *Journal of Magnetic Resonance* (1969) 1986;67(2):258 – 266. <http://www.sciencedirect.com/science/article/pii/0022236486904336>.
- [2] Hennig J, Nauerth A, Friedburg H. RARE imaging: A fast imaging method for clinical MR. *Magnetic Resonance in Medicine* 1986;3(6):823–833. <https://onlinelibrary.wiley.com/doi/abs/10.1002/mrm.1910030602>.
- [3] Carr HY. Steady-State Free Precession in Nuclear Magnetic Resonance. *Phys Rev* 1958 Dec;112:1693–1701. <https://link.aps.org/doi/10.1103/PhysRev.112.1693>.
- [4] Jin KH, Unser M, Yi KM. Self-Supervised Deep Active Accelerated MRI. *arXiv 2019;arXiv eprint: 1901.04547*.
- [5] Weiss T, Vedula S, Senouf O, Bronstein A, Michailovich O, Zibulevsky M. Learning Fast Magnetic Resonance Imaging. *arXiv 2019;arXiv eprint: 1905.09324*.
- [6] Sherry F, Benning M, los Reyes JCD, Graves MJ, Maierhofer G, Williams G, et al. Learning the Sampling Pattern for MRI. *arXiv 2019;arXiv eprint: 1906.08754*.
- [7] Bahadir CD, Dalca AV, Sabuncu MR. Learning-based Optimization of the Under-sampling Pattern in MRI. *arXiv 2019;arXiv eprint: 1901.01960*.
- [8] Weiss T, Senouf O, Vedula S, Michailovich O, Zibulevsky M, Bronstein A. PILOT: Physics-Informed Learned Optimal Trajectories for Accelerated MRI. *arXiv 2019;arXiv eprint: 1909.05773*.

- [9] Zhu, AUTOMated pulse SEquence generation (AUTOSEQ) using Bayesian reinforcement learning in an MRI physics simulation environment; 2018. <http://archive.ismrm.org/2018/0438.html>.
- [10] Walker-Samuel, Using deep reinforcement learning to actively, adaptively and autonomously control a simulated MRI scanner; 2019. <https://cds.ismrm.org/protected/19MPresentations/abstracts/0473.html>.
- [11] Shin F, Deep reinforcement learning designed RF pulse; 2019. <https://index.mirasmart.com/ISMRM2019/PDFfiles/0757.html>.
- [12] Zhu, AUTOMated pulse SEquence generation (AUTOSEQ) and neural network decoding for fast quantitative MR parameter measurement using continuous and simultaneous RF transmit and receive; 2019.
- [13] Paszke A, Gross S, Chintala S, Chanan G, Yang E, DeVito Z, et al. Automatic differentiation in PyTorch. NIPS-W 2017;.
- [14] Abadi M, Agarwal A, Barham P, Brevdo E, Chen Z, Citro C, et al., TensorFlow: Large-Scale Machine Learning on Heterogeneous Systems; 2015. <http://tensorflow.org/>, software available from tensorflow.org.
- [15] Layton KJ, Kroboth S, Jia F, Littin S, Yu H, Leupold J, et al. Pulseseq: A rapid and hardware-independent pulse sequence prototyping framework. *Magnetic Resonance in Medicine* 2017;77(4):1544–1552. <https://onlinelibrary.wiley.com/doi/abs/10.1002/mrm.26235>.
- [16] Kingma DP, Ba J. Adam: A Method for Stochastic Optimization. arXiv 2014;arXiv eprint: 1412.6980.
- [17] Hennig J SK Weigel M. Multiecho sequences with variable refocusing flip angles: optimization of signal behavior using smooth transitions between pseudo steady states (TRAPS). *Magn Reson Med* 2003;49:527–535.
- [18] Li Y. Deep Reinforcement Learning: An Overview. arXiv 2017;arXiv, eprint: 1701.07274.
- [19] Bertsekas DP. Reinforcement learning and optimal control. Athena Scientific 2019;1.
- [20] Knoll F, Hammernik K, Zhang C, Moeller S, Pock T, Sodickson DK, et al. Deep Learning Methods for Parallel Magnetic Resonance Image Reconstruction. arXiv 2019;arXiv eprint: 1904.01112.
- [21] Virtue P, Stella XY, Lustig M. Better than real: Complex-valued neural nets for MRI fingerprinting. In: 2017 IEEE International Conference on Image Processing (ICIP) IEEE; 2017. p. 3953–3957.
- [22] Ma D, Gulani V, Seiberlich N, Liu K, Sunshine JL, Duerk JL, et al. Magnetic resonance fingerprinting. *Nature* 2013 Mar;495:187. <https://doi.org/10.1038/nature11971>.
- [23] Poorman ME, Martin MN, Ma D, McGivney DF, Gulani V, Griswold MA, et al. Magnetic resonance fingerprinting Part 1: (Potential) uses, current challenges, and recommendations. *Journal of Magnetic Resonance Imaging* 2019;<https://onlinelibrary.wiley.com/doi/abs/10.1002/jmri.26836>.
- [24] McGivney DF, Boyacıoğlu R, Jiang Y, Poorman ME, Seiberlich N, Gulani V, et al. Magnetic resonance fingerprinting review part 2: Technique and directions. *Journal of Magnetic Resonance Imaging* 2019;n/a. <https://onlinelibrary.wiley.com/doi/abs/10.1002/jmri.26877>.
- [25] Kördörfer G, Kirsch R, Liu K, Pfeuffer J, Hensel B, Jiang Y, et al. Reproducibility and Repeatability of MR Fingerprinting Relaxometry in the Human Brain. *Radiology* 2019;292(2):429–437. <https://doi.org/10.1148/radiol.2019182360>.
- [26] Cohen O, Rosen MS. Algorithm comparison for schedule optimization in MR fingerprinting. *Magnetic resonance imaging* 2017;41:15–21.
- [27] Zhu B, Liu JZ, Cauley SF, Rosen BR, Rosen MS. Image reconstruction by domain-transform manifold learning. *Nature* 2018;555(7697):487.
- [28] Ravi KS, Potdar S, Poojar P, Reddy AK, Kroboth S, Nielsen JF, et al. Pulseseq-Graphical Programming Interface: Open source visual environment for prototyping pulse sequences and integrated magnetic resonance imaging algorithm development. *Magnetic resonance imaging* 2018;52:9–15.

6 | SUPPORTING INFORMATION

6.1 | Forward model

The forward process of the image acquisition process that we use is outlined in an Algorithm box below.

Algorithm 1: Initialize: \mathbf{m} to initial magnetization state: $\mathbf{m} = \mathbf{m}_0 = \hat{\mathbf{e}}_z * PD$, where $PD \in \mathbb{R}_{vox}^N$ is a proton density vector

```

for  $r \leftarrow 0 : N_{rep}$  do
  for  $a \leftarrow 0 : N_{actions}$  do
     $\mathbf{m} = FLIP_y(\alpha_{r,a} * B1^+, \phi_{r,a})\mathbf{m}$ 
     $\mathbf{m} = RELAX(\Delta t_{r,a})\mathbf{m} + (1 - RELAX(\Delta t_{r,a}))\mathbf{m}_0\hat{\mathbf{e}}_z$ 
     $\mathbf{m} = FREEPRECESS(\Delta t_{r,a})\mathbf{m}$ 
     $\mathbf{m} = GRADPRECESS(\mathbf{g}_{x,r,a}, \mathbf{g}_{y,r,a})\mathbf{m}$ 
     $s_{r,a} = ADC(d_{r,a})\mathbf{m}_{transverse} + \epsilon$ 
  end
end

```

Output: signal $\mathbf{s} \in \mathbb{R}^{N_{rep} \times N_{actions} \times 2}$ (complex-valued but stored in a real number type array)

At each sequence repetition, a loop over $N_{actions}$ steps is performed. Each *action* step consists of the temporal concatenation of the following linear operators:

1. *FLIP* operator performs a rotation of magnetization vector by α degrees around a rotation axis vector in transverse plane, whose orientation is determined by RF pulse phase ϕ . $B1^+ \in \mathbb{R}^{N_{vox}}$ vector rescales the flip angles to represent an effective variation of flip angles in real measurement due to non-uniformity of excite field.

2. *RELAX* diagonal operator shrinks the components of magnetization vector according to T1 and T2 relaxation values, and restores the longitudinal component back to initial value. The duration of relaxation is determined by a $\Delta t \in \mathbb{R}^{N_{actions} \times N_{rep}}$ parameter. As such, *RELAX* operator implements numerical solution to Bloch equations.

$$RELAX(\Delta t) = \begin{pmatrix} \exp(-\frac{\Delta t}{T_2}) & 0 & 0 \\ 0 & \exp(-\frac{\Delta t}{T_2}) & 0 \\ 0 & 0 & \exp(-\frac{\Delta t}{T_1}) \end{pmatrix}$$

3. *FREEPRECESS* operator rotates a magnetization vector around the Z axis by an angle dictated by the local susceptibility-dependent field inhomogeneities as well as global B0 variations due to shim imperfections. Both *RELAX* and *FREEPRECESS* operators are influenced by a time variable Δt , which is one of the optimized parameters. Using a time variable to control the durations of relaxation and free precession allows to avoid expensive simulations on a fixed time interval regular temporal grids. This results in smaller number of parameters to be optimized and minimal number of tensor-tensor operations.

4. *GRADPRECESS* operator models frequency and phase encoding as well as transverse magnetization spoiling. *GRADPRECESS* operator rotates a magnetization vector around the Z axis subject to linear magnetic field gradient ramps imposed by the gradient system of the scanner. Importantly, we use a gradient moment as a parameter, which couples the effective gradient strength at each time point together with duration of gradient application. As such, \mathbf{g} parameters equal to a temporal integral over waveform of applied gradient current.

5. *ADC* performs the integration of transverse components of magnetization vector subject to ADC-open-closed indicator variable $\mathbf{d} \in \{0, 1\}^{N_{actions}}$, and returns a vector with two components, which are conventionally treated as real and

imaginary parts of the measured signal. Furthermore, we assume that the signal s is affected by an additive Gaussian noise ϵ with zero mean and σ variance (same at each voxel). The noise component represents thermal spin and RF noise in the simulation.

The simulation setup presented above allows implementation of a wide variety of MR sequences. It is important to note that although each *action* is defined as five concatenated operators, depending on the actual values of sequence parameters some of these operators can be skipped from simulation, speeding up the forward pass. I.e., if flip angles at certain repetition/*action* are zero the respective *action* block omits *FLIP* operator from the computation chain.

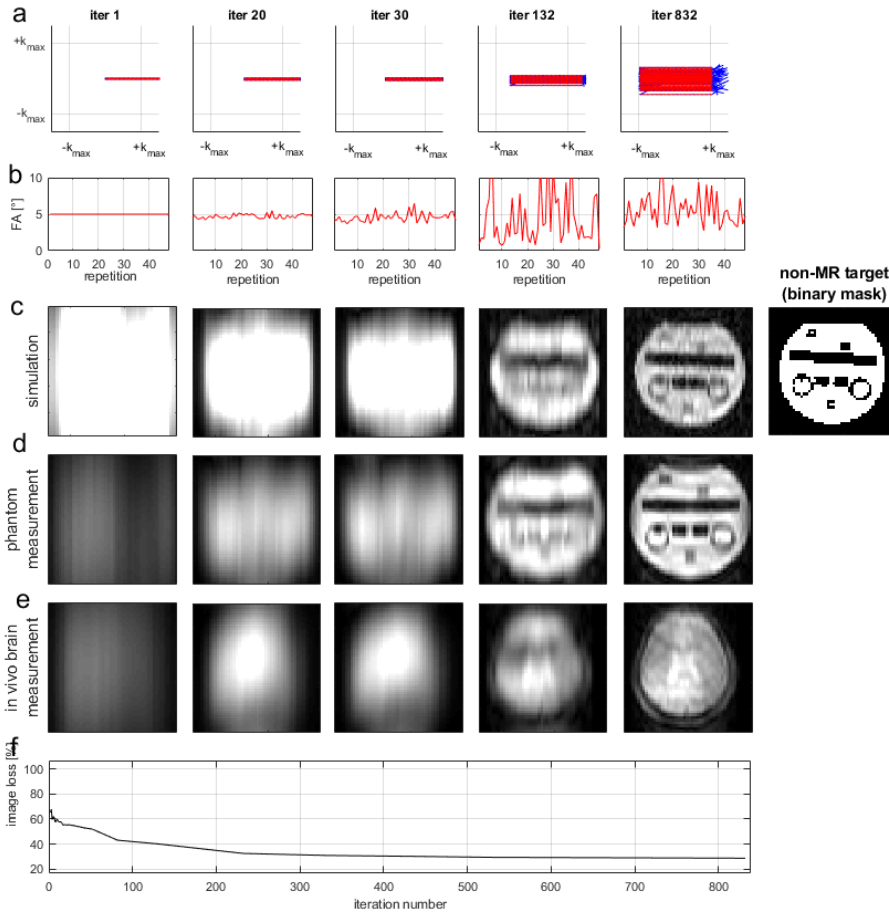
6.2 | Joint optimization of sequence and neural network for T1 Mapping

For the T1 mapping approach, shown in Figure 7 in the main text, a sparse synthetic database was used as training dataset. The training dataset consist of ten T1 maps with matrix size 32x32. For each target sample a non-zero PD rectangle with matrix size 12x12 at varying spatial location is defined. Each voxel inside the rectangle has randomly assigned PD, T1, T2 and B0 values in range of (0 – 1.5), (0.3 – 6.1) s, (0 – 3.8) s, (-60 – 60) Hz, respectively. A three-hidden-layer multilayer perceptron is used for T1 quantification, which as well implemented in Torch [13]. To induce non-linearity ReLu [1] is used as activation function between each layer. The neural network takes as input the signal evolution of a single voxel for 10 measurements at different TI and Trec. The output or prediction is the corresponding T1 value of the voxel. The chosen optimizer for NN training is Adam. For T1 mapping a 180 deg inversion prepared 2D transient gradient- and RF-spoiled centric reordered GRE sequence is used with matrix size 32, TR = 15 ms, TE = 8ms, FA = 5 deg, repeated 10 times with varying TI and Trec. TI and Trec times are optimized to find the best sequence for T1 mapping and are initialized with 0. The optimization process starts by initially training the neural network for 5000 iterations with simulated images from the initial sequence. Afterwards, optimization of the sequence and neural network are alternating after 50 and 1000 iterations, respectively. Between each switch from sequence optimization to NN optimization a forward process runs with new optimized sequence parameters to update the simulated images. In total 500 iterations of sequence optimization are performed. The standard inversion recovery (rightmost column in Figure 7) was evaluated both with a conventional fit, but as well using a neural network. The conventional fit data was not shown, as it had bad performance especially for long T1 values, so the comparison to neural network evaluation appeared more fair.

6.3 | Non-MR target

Supporting Figure S1 shows that *MRzero* can learn image encoding even given non-MR input. The task here is identical to the task of Figure 2 in the main text except the target is only a binary mask of the same phantom. It is important to note that in this experiment we do not attempt to reconstruct a binary mask as faithfully as possible using the learned sequence. The task is practically impossible and the target can never be matched perfectly. The goal is to rather show that optimization process itself can be driven with such a weak generic target as a segmentation mask.

This experiment refers to case I) in Figure 1 of the main text, without having a neural network enabled yet. However, generation of segmentation would be possible as well with the current approach using reconstruction case II) or case III) of Figure 1.

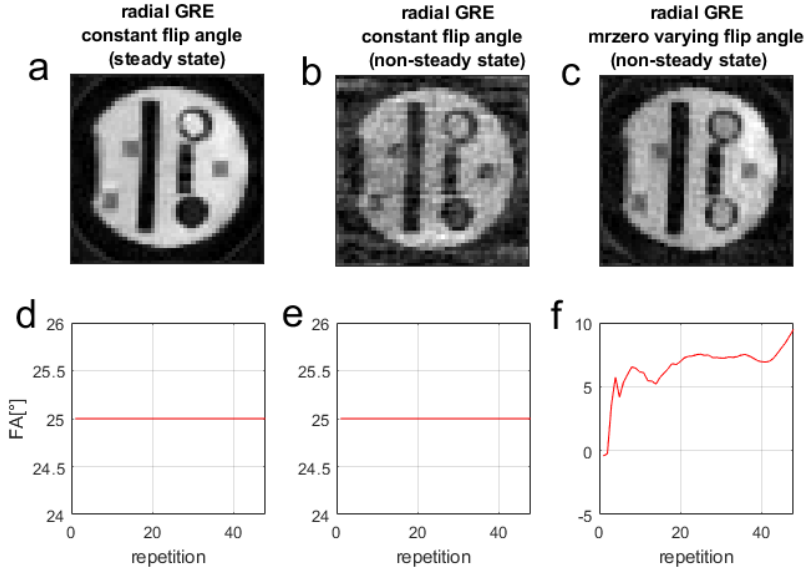


Supporting Figure S1: Full gradient and RF optimization using only a segmentation mask of the phantom as a target. Row a: k-space sampling at different iterations, Row b: flip angles over sequence repetitions. Row c: simulation-based reconstruction at different iterations 1, 20 30, 132 and 832. row d: phantom measurement, row e: in vivo brain scan. Row f: training error curve.

6.4 | radial MR

Beyond SAR optimization, varying flip angles also allow to remove artifacts in transient sequences due to signal decay during readout, a major problem for radial sequences. Supporting Figure S2 shows the artifact in a transient radial scan, and how *MRzero* is able to compensate for the transient decay by adjusting the flip angle accordingly: the transient decay of magnetization is compensated by a variable flip angle acquisition with increasing flip angles.

Please note that the radial reconstruction requires an iterative adjoint reconstruction approach, which was used as



Supporting Figure S2: A radial GRE sequence driven in steady state (a) employing constant flip angles (d). When this same sequence is used in transient state, reconstruction artifacts due to the decay of the magnetization are observed (b). MRzero is able to compensate this by finding a variable flip angle pattern (f) that compensates for the signal decay yielding an artifact free image (c). Target sequence: radial gradient- and RF-spoiled GRE, target matrix size 48, TR = 20 ms, TE = 3 ms, FA=25°.

described in the following. The adjoint-based reconstruction we presented in this work can be seen as a special case of a more general iterative procedure. Consider a general system of equations $Ax = b$. The system can be solved for x using an iterative gradient descent:

$$x_{n+1} = x_n - \alpha \frac{\partial \|Ax_n - b\|_2^2}{\partial x_n} = x_n - 2\alpha A^H(Ax_n - b); \quad x_0 = 0 \quad (2)$$

where α is a step size, determining the convergence rate of the gradient descent. To make a connection to formalism of our paper, note that b is a signal output by the scanner function, A is the encoding matrix determined by spatial encoding gradients, and x is the image in spatial domain that we want to reconstruct. In case of plain adjoint reconstruction (used in most experiments in this work), we use a first order solution: $x_1 = -2\alpha A^H(-b) \approx A^H b$. In Cartesian, fully sampled, uniform acquisitions such solutions is adequate, since Hermitian of encoding matrix approximately equal to its inverse, the eigenvalue spectrum of the matrix A is uniform and unitary, and the system is invertible. In case of non-Cartesian acquisitions with variable density the eigenvalues of the encoding matrix A can be such that condition number defined as a ratio of largest to smallest eigenvalue is large, and thus convergence is slow requiring many iterations. For example, in case of radial acquisitions the center of the k-space is oversampled, meaning that the eigenvalues corresponding to low spatial frequency eigenvectors are large compared to the rest of the eigenvalues. In such regime, a first order transpose solution will appear blurry, being composed mostly of low-frequency components. Thus, in case of non-Cartesian measurements we resort to higher order iterations, in our experiment with radial acquisitions $n = 10$. Using Torch-based autodifferentiation we can still conveniently estimate and back-propagate all variables through

entire chain of iterations. This results in even more non-linear complicated form of the the objective function, however, interestingly we did not observe the convergence to be any worse compared to the first order solution.

7 | REFERENCES

[1] Hahnloser, R.; Sarpeshkar, R.; Mahowald, M. A.; Douglas, R. J.; Seung, H. S. (2000). "Digital selection and analogue amplification coexist in a cortex-inspired silicon circuit". *Nature*. 405: 947–951. doi:10.1038/35016072.